Cranial bone histology of *Metoposaurus krasiejowensis* (Amphibia, Temnospondyli) from the Late Triassic of Poland

Kamil Gruntmejer Corresp., [1, 2] , **Dorota Konietzko-Meier** [1, 2, 3] , **Adam Bodzioch** [1]

[1] Department of Biosystematics, University of Opole, Opole, Poland
[2] European Centre of Palaeontology, University of Opole, Opole, Poland
[3] Steinmann Institute, University of Bonn, Bonn, Germany

Corresponding Author: Kamil Gruntmejer
Email address: gruntmejerkamil@gmail.com

In this study, 21 skull bones of *Metoposaurus krasiejowensis* from the Late Triassic of Poland were investigated histologically. Dermal bones show a diploë structure, with an ornamented external surface. The ridges consist of mostly well vascularized parallel-fibered bone; the valleys are built of an avascular layer of lamellar bone. The thick middle region consists of cancellous bone, with varying porosity. The thin and less vascularized internal cortex consists of parallel-fibered bone. The numerous Sharpey's fibers and ISF are present in all bones. The cyclicity of growth is manifested as an alternation of thick, avascular annuli and high vascularized zones as well as a sequence of resting lines. The detailed histological framework of dermal bones varies even within a single bone; this seems to be related to the local biomechanical loading of the particular part of the skull. The dynamic processes observed during the ornamentation creation indicate that the positions of the ridges and grooves change during growth and could be a specific adaptation to changing biomechanical conditions and stress distribution during bone development. In the supratemporal, the cementing lines show that the remodeling process could be involved in the creations of sculpture. The common occurrence of ISF suggests that metaplastic ossification plays an important role during cranial development. Endochondral bones preserved the numerous remains of calcified cartilage. This indicates that ossification follows a pattern known for stereospondyl intercentra, with relatively slow ossification of the trabecular part and late development of the periosteal cortex. The large accumulation of Sharpey's fibers in the occipital condyles indicates the presence of strong muscles and ligaments connecting the skull to the vertebral column.

Cranial bone histology of *Metoposaurus krasiejowensis* (Amphibia, Temnospondyli) from the Late Triassic of Poland

Kamil Gruntmejer[1,2,*], Dorota Konietzko-Meier[1,2,3], Adam Bodzioch[1]

[1] Opole University, Department of Biosystematics, Laboratory of Palaeobiology, Oleska 22, 45-052 Opole, Poland

[2] Opole University, European Centre of Palaeontology, Oleska 48, 45-052 Opole, Poland

[3] University of Bonn, Steinmann Institute, Nussallee 8, 53115 Bonn, Germany

[*]gruntmejerkamil@gmail.com

* - corresponding author

ABSTRACT

In this study, 21 skull bones of *Metoposaurus krasiejowensis* from the Late Triassic of Poland were investigated histologically. Dermal bones show a diploë structure, with an ornamented external surface. The ridges consist of mostly well vascularized parallel-fibered bone; the valleys are built of an avascular layer of lamellar bone. The thick middle region consists of cancellous bone, with varying porosity. The thin and less vascularized internal cortex consists of parallel-fibered bone. The numerous Sharpey's fibers and ISF are present in all bones. The cyclicity of growth is manifested as an alternation of thick, avascular annuli and high vascularized zones as well as a sequence of resting lines. The detailed histological framework of dermal bones varies even within a single bone; this seems to be related to the local biomechanical loading of the particular part of the skull. The dynamic processes observed during the ornamentation creation indicate that the positions of the ridges and grooves change during growth and could be a specific adaptation to changing biomechanical conditions and stress distribution during bone development. In the supratemporal, the cementing lines show that the remodeling process could be involved in the creations of sculpture. The common occurrence of ISF suggests that metaplastic ossification plays an important role during cranial development. Endochondral bones preserved the numerous remains of calcified cartilage. This indicates that ossification follows a pattern known for stereospondyl intercentra, with relatively slow ossification of the trabecular part and late development of the periosteal cortex. The large accumulation of Sharpey's fibers in

the occipital condyles indicates the presence of strong muscles and ligaments connecting the skull to the vertebral column.

Keywords:
Temnospondyli, dermal bones, skull, histology, microanatomy

INTRODUCTION

Metoposaurids were large, up to 3 meter long, late Triassic Temnospondyli with a strongly dorso-ventrally flattened body, adapted to aquatic life. The most characteristic and best known part of the *Metoposaurus* skeleton is the extremely flat and parabolic skull with anteriorly located orbits (e.g. Schoch & Milner, 2000). The temnospondyl skull functionally represents one skeletal element; however, anatomically, it is a conglomerate of numerous bones varying in shape and thickness, having various functions and biomechanical loads (i.e. Fortuny et al., 2011, Fortuny et al., 2012).

The flat bones of the skull represent the dermal bones that develop via direct transformation of preexisting connective tissue (Francillon-Vieillot et al., 1990). The external surface of the dermal bones is characteristically ornamented. A network of raised, reticulate ridges that enclose approximately flat-bottomed, interlocking, polygonal cells is the most common type. The vast majority of these cells are four-, five-, or six-sided, creating a honeycomb- or waffle-iron-like texture. In some temnospondyls, this is essentially the only texture present. The second texture type comprises raised, parallel to sub-parallel ridges separated by round-bottomed grooves (Rinehart & Lucas, 2013). The function of the ornamentation is still unclear. The best supported hypotheses suggest that they increase the

surface area for skin supports, increase the strength of the bone, protect blood vessels or assist in thermal exchange (summarized in Coldiron, 1974; Witzmann, 2009; Rinehart & Lucas, 2013; Clarac et al. 2015, 2016).

The histology of amniote osteoderms is well known and studied in detail for several groups (e.g. Scheyer & Sander, 2004; Vickaryous & Sire, 2009; Buffrénil et al., 2011; Burns et al., 2013; Scheyer et al., 2014; Cerda et al., 2015 and further references in all). The histology of temnospondyl dermal bones is less known and was first described by Gross (1934), who provided a short description of the skull bones of *Mastodonsaurus*, *Metoposaurus* and *Plagiosternum*, and recognized that the dermal bones exhibit a diploë structure. Later histological studies on the dermal bones in Temnospondyli have focused mainly on morphology and vascular network and collagen fiber organization (Bystrow, 1947; Enlow & Brown, 1956; Coldiron, 1974; de Ricqlès, 1981; Castanet *et al*, 2003; Scheyer, 2007), and were limited only to a few taxa. The systematic studies of dermal bones within numerous tetrapod taxa were provided by Witzmann (2009) and de Buffrénil et al. (2016). Up until now, the dermal bones of *Metoposaurus* have not been studied in detail histologically. The only record of the histological description of *Metoposaurus diagnosticus* dermal bone was given by Gross (1934), later re-described by Witzmann (2009). However, it is unclear if the illustrated section was derived from the skull or the pectoral girdle, or even if the published bone fragment belongs to *Metoposaurus* at all.

The main goal of this study is to present a detailed description of the histology of dermal and endochondral bones from one skull of *Metoposaurus krasiejowensis* (Sulej, 2002), and determine, if possible, the tendencies and variability of the histological framework. Moreover,

the value of the dermal bones for the skeletonchronological analyses, the ossification modes of the skull, and origin of the sculpture will be evaluated.

MATERIAL AND METHODS

Material. The skull (UOPB 01029; 40 cm in length) of *Metoposaurus krasiejowensis* was studied histologically (Figs. 1 and 2). The roof side of the skull was almost completely preserved, whereas on the palatal side only the fragments of the vomer, parasphenoid, pterygoids, quadrates and exoccipitals were preserved. The species discovered in Poland was originally described as *Metoposaurus diagnosticus krasiejowensis* Sulej, 2002, the subspecies of an older *Metoposaurus diagnosticus* (Meyer, 1842). Brusatte *et al*. (2015) recommended against using the subspecies for the German *M. diagnosticus diagnosticus* (von Meyer, 1842) and the Polish *M. diagnosticus krasiejowensis*, suggesting instead to separate them at the species level as *M. diagnosticus* and *M. krasiejowensis*. That taxonomy is followed in this study.

Locality. The examined material comes from the famous locality in Krasiejów where a large number of disarticulated skeletons were discovered in the Upper Triassic (Keuper), fine-grained, continental sediments. The bones can be found in two main bone-bearing horizons, referred to as the lower and the upper horizon (Dzik & Sulej, 2007). The lower horizon was deposited on an alluvial plain during a catastrophic mud-flow event (Bodzioch & Kowal-Linka, 2012). The skull presented here was excavated from the less than 1 m thick lower bone-bearing layer, which is very rich in *Metoposaurus krasiejowensis* remains, also accompanied by relatively a high diversified fossil assemblage. Vertebrates are represented by a second temnospondyl, *Cyclotosaurus intermedius* Sulej & Majer, 2005, a phytosaur (*Palaeorhinus*; see

Dzik, 2001), the typical terrestrial tetrapod aetosaur *Stagonolepis olenkae* Sulej, 2010, pterosaurs (Dzik & Sulej, 2007), sphenodonts and other small tetrapods (Dzik & Sulej, 2007), as well as fishes (dipnoans described recently by Skrzycki, 2015, and various actinopterygian and chondrichthyan species). Invertebrates, such as unionid bivalves (Dzik et al., 2000; Skawina & Dzik, 2011; Skawina, 2013), cycloids (Dzik, 2008), spinicaudatan crustaceans (Olempska, 2004), fresh-water ostracods (Olempska, 2004, 2011), and some gastropods are also very common. The upper horizon is restricted to lenses cemented with calcium carbonate, interpreted as a meander deposit (e.g. Gruszka and Zieliński, 2009). It is dominated by strictly terrestrial animals including *Stagonolepis* and the primitive dinosauromorph *Silesaurus opolensis* Dzik, 2003. Aquatic vertebrates such as amphibians and phytosaurs are less common compared to their abundance in the lower horizon. Apart from that, one fragmentary specimen of the rauisuchian *Polonosuchus silesiacus* (Brusatte et al., 2010) was excavated between the upper and lower horizons.

According to complex stratigraphic studies of the Upper Silesian Keuper, the bone-bearing beds were deposited in the early Norian times (Racki & Szulc, 2014; Szulc et al., 2015a, b). However, biochronological data uphold the Late Carnian age (e.g. Dzik & Sulej 2007; Lucas et al. 2007; Lucas, 2015).

Methods. The skull was sectioned in 20 planes (Fig. 2), and the thin sections were prepared according to standard petrographic procedures (Chinsamy and Raath, 1992) in the Laboratory of the University of Poznan (Poland) and in the laboratory of Steinmann Institute (University of Bonn, Germany). The thin sections were ground and polished to a thickness of about 60-80 μm using wet SiC grinding powders (SiC 600, 800). Subsequently, the thin sections were studied under a LEICA DMLP light microscope in plane and cross polarized light.

137 The histological nomenclature follows, with an exception for annuli, Francillon-Vieillot
138 et al. (1990) and Witzmann (2009). According to Francillon-Vieillot et al. (1990), the annual
139 growth cycle consists of a thick, fast growing zone, a thin, slow growing annulus, and a Line of
140 Arrested Growth (LAG). In this study, the term zone is used as in its traditional meaning, for the
141 highly vascularized layer with lower organization of collagen fibers. The term annulus, however
142 (not following Francillon-Vieillot et al., 1990), refers to the less-vascularized bone with higher
143 organization of collagen fibers, but usually similar in thickness as a zone. In the studied material,
144 no clear LAGs can be observed. Instead, adjacent to the annuli, numerous lines are present. To
145 avoid nomenclatural problems, all lines representing the cessation of growth are referred to in
146 this study as resting lines, without determination of whether they occur annually or not
147 (Konietzko-Meier & Sander, 2013; also see discussion).
148 In the thin sections, the average thickness of the entire bone and of each layer was
149 estimated, expressed as an arithmetical average from three measurements of the thickness of the
150 entire bone/layer. The thickness of the external layer was measured three times on the distance
151 between the border line with middle region and the bottom of valleys, and three times as the
152 distance between the border line (remodeling front) with middle region and the top of ridges. The
153 mathematical average was calculated from these measurements. The minimum and maximum
154 thicknesses represent the lowest and largest measurement, respectively, for each described layer.
155 For the estimation of the ratio between the three components (E – external cortex, M – middle
156 region, I – internal cortex; E:M:I), the average thickness of the external cortex was taken as one
157 and then proportionately the value for middle region and internal cortex were calculated. Note
158 that the internal cortex of dermal bone is oriented to the visceral surface of the body. Thus, in the
159 parasphenoid, pterygoid and vomer, the external cortex is then oriented ventrally.

A detailed description of each bone is presented in the Supplementary Material.

RESULTS

Microanatomy of dermal bones

Most dermal bones of the skull are flat plates. Only the premaxillae and maxillae possess a more complicated shape (Fig. 3). The premaxilla is built up of three branches: the dental shelf, the alary process (Schoch, 1999), and the vomeral process, which connects the dental shelf to the vomer (Fig. 3A). The maxilla is built up from two branches: the dorsal one with an ornamented external cortex, and the ventral branch with the dental shelf (Fig. 3B).

The dermal bones show clear diploë (Fig. 4). The external cortex of the skull-roof bones created variably ornamentations built from a combination of grooves or tubercles and ridges (Tab. 1, Fig. 1), respectively visible in the cross-section as valleys and ridges (Fig. 4A). The thickness of the flat bones varies from under 1.5 to over 10 millimeters (Tab. 1), with different proportions between the particular layers. No constant relation can be observed between the thickness of the external cortex and the thickness of the entire bone. However, the external cortex of the tabular and postparietal, the two most massive bones, is clearly thicker than in other bones (Tab. 1). The relatively thin squamosal 2, with an average thickness of only about three mm, developed an external cortex which takes up almost half of the bone thickness (Tab. 1). The largest part of the bone almost always consists of the middle region (which is about two times thicker as the external cortex), with the exception of squamosal 2, where the middle region is the thinnest (Tab. 1). The internal cortex is the thinnest of the three layers and composes usually 40% to 90% of the thickness of the external cortex, with the exception of the pterygoid (Tab. 1).

183

184 **General histology of dermal bones**

185 **External cortex**. In all sections, the external cortex consists of parallel-fibered bone,
186 whereas in the valleys lamellar bone often occurs (Fig. 4B and C). The elongated osteocyte
187 lacunae with branched canaliculi in the bone matrix are numerous (Fig. 5A). Vascular canals are
188 mostly longitudinally oriented (Fig. 5A, B). The degree of vascularization varies from relatively
189 low in the premaxilla and frontal, moderate in the maxilla and prefrontal, to highly vascularized
190 in the jugal, postorbital, parietal, squamosal, quadratojugal, vomer and parasphenoid. In the
191 nasal, postparietal, postfrontal, tabular and supratemporal, numerous vascular canals within the
192 ridges are visible, which are arranged in rows parallel to the bony surface, whereas the valleys
193 are avascular. The external cortex is dominated by simple vascular canals and primary osteons.
194 In some bones (nasal, lacrimal, prefrontal, tabular, squamosal, vomer and parasphenoid), many
195 secondary osteons and a few erosion cavities are visible in the transition region to the middle
196 layer (for details see the Supplementary Material).

197 Typical for the external cortex are distinct collagen fibers (Fig. 5C, D). In the premaxilla,
198 maxilla, nasal, lacrimal, jugal, postorbital, postparietal, and quadratojugal, well-mineralized
199 Sharpey's fibers can be observed, which are relatively short but numerous, and sometimes
200 packed densely in bundles. In the prefrontal, frontal, postfrontal, parietal, supratemporal,
201 squamosal, tabular and vomer, Sharpey's fibers are rare and occur mostly in the deeper parts of
202 the sculptural ridges (Fig. 5C). In the parasphenoid and pterygoid, Sharpey's fibers cannot be
203 observed. In some bones (jugal, postorbital, postfronat, postparietal, tabular), thick fibers create
204 Interwoven Structural Fibers (ISF) (Fig. 5D). In the postparietal, a structure resembling

metaplastic bone is constructed from longitudinally and transversely oriented structural fibers is visible (Fig. 5 D).

Growth marks are expressed in two ways. In the ridges of the lacrimal, frontal, jugal, postfrontal, tabular, quadratojugal and squamosal 2, they are manifested as a sequence of thin resting lines (Fig. 5E). In the quadratojugal, two thick annuli built up of lamellar bone alternate with two highly vascularized zones (Fig. 5F).

In the postfronal, squamosal 1, supratemporal, tabular, jugal and quadratojugal, the alternations of valleys and ridges are preserved. The remains of older valleys are filled with the highly vascularized tissue, which then constructed the ridges of the next generation (Fig. 5G). In the supratemporal, the cementing line is visible (Fig. 5H).

Middle region. The external cortex changes gradually into the cancellous middle region. The simple vascular canals and primary osteons, of various shapes, are mostly located next to the border between the middle and external regions. A significant part of the middle region is strongly remodeled. The few large erosion cavities (up to 2000 μm in diameter) are present in the premaxilla, nasal, lacrimal, jugal, prefrontal, postparietal, squamosal 1, quadratojugal and all studied bones from the palatal side of the skull. The most highly remodeled middle region occurs in the vomer, where the trabeculae are extremely reduced and erosion cavities in some areas exceed 3000 μm in length (Fig. 6A). In the lacrimal and prefrontal, erosion cavities reach up to the external cortex. The maxilla is dominated by numerous, medium-sized erosion cavities. In the postfrontal, parietal and supratemporal, erosion cavities are small (less than 500 μm in diameter). In the postfrontal they appear sporadically, whereas they are numerous in the parietal and supratemporal (Fig. 6B). The middle region in the tabular and squamosal 2 does not show

the typical trabecular structure. Intensive remodeling is visible; however, the tissue is relatively compact, almost without erosion cavities (Fig. 6C).

Internal cortex. The internal cortex consists of parallel-fibered to lamellar bone. The degree of vascularization varies from very low and almost avascular in the parietal, postfrontal, supratemporal and squamosal, low in the premaxilla, prefrontal, nasal, and postparietal, moderate in the maxilla, frontal, vomer and parasphenoid, to high in the lacrimal, jugal, postorbital and quadratojugal (Fig. 6D-F). Osteocyte lacunae, showing slightly elongated shapes, are very common. Growth marks are visible in the form of resting lines and a sequence of zones and annuli. The number of lines varies from four in the postfrontal and parietal, three in the postparietal, supratemporal and jugal, to two in the nasal (Fig. 6D). In the parasphenoid, well developed zones and annuli can be observed (Fig. 6G). Zones are built of thick, well vascularized layers, whereas annuli are represented by thinner, avascular layers. The numerous Sharpey's fibers packed in bundles are visible in the tabular and vomer.

Endochondral bones

Quadrate. The partially preserved and well-vascularized cortex consists of parallel-fibered and lamellar bone (Fig. 7A, B). The simple vascular canals occur sporadically, and secondary osteons are more common (Fig. 7A, B). The Sharpey's fibers are very short and occur only in the subsurface parts of the cortex. The elongated osteocyte lacunae are present mainly within the lamellar bone, which outlines the osteons. They do not possess canaliculi. Growth marks cannot be observed.

248 The central region consists of spongiosa and is characterized by large pore spaces and irregular
249 trabeculae (Fig. 7C), which contain clumps of calcified cartilage (see also the Supplementary
250 Material).

251 **Exoccipital.** The cortex consists of parallel-fibered bone and is relatively well-
252 vascularized (Fig. 7D). The simple vascular canals are few in number (Fig. 7E, F) and located
253 only in the outermost part of the cortex. The secondary osteons are more frequent (Fig. 7D).
254 Well-mineralized, densely packed bundles of Sharpey's fibers are common and can be seen
255 throughout the entire cortex (Fig. 7D, E). In the exoccipital, the Sharpey´s fibers are most
256 abundant and pronounced among all examined bones. Rounded osteocyte lacunae are numerous.
257 Growth marks are absent.

258 The central region consists of an irregular network of bony trabeculae, with large pore
259 spaces between them (Fig. 7G). In the medial parts of the bone tissue, where trabeculae are
260 poorly developed, accumulations of calcified cartilage are quite common (Fig. 7H).

261

262 **DISCUSSION**

263

264 **The histological variability.** Witzmann (2009) investigated fragments of dermal bones
265 from 20 taxa and concluded that for every taxon, the bone microanatomy and histology were
266 consistent. Intraspecific variability of the histology of dermal bones was only observed in
267 *Mastodonsaurus giganteus* and *Plagiosternum granulosum*, concerning the degree of
268 vascularization and remodeling of the bone (Witzmann, 2009).

269 Nevertheless, in the *Metoposaurus krasiejowensis* skull, the variability is high and can be
270 seen at both the microanatomical and histological levels. The bones pose variable thicknesses,

different proportions between the layers, variations in the vascularization systems, tissue organizations, the presence and organization of Sharpey's fibers, degree of remodeling, and growth patterns (see also the Supplementary Material for detailed descriptions). The combination of these characters shows that nearly very sectioning-plane in the skull represents a unique framework. The transition between the "histological types" is fluid. The jugal and postorbital, sectioned in the suture region, represent the same microanatomical and histological framework (Figs. 2 j and po, 3F; Tab. 1), whereas the squamosal sectioned in the frontal part of the bone (Fig. 2, sq1) and next to the otic notch (Fig. 2, sq2) show different architectures on both microanatomical and histological levels (Figs. 3K, L). This suggests that the histological framework is not specifically bone-limited, but seems to be related to the specific area of the skull. That is, it depends on the growth of the entire skull and each bone separately, the local biomechanical loading on a particular part of the skull, or a combination of both. Fortuny et al. (2012), based on a Finite Elements Analysis, showed that the hypothetical biomechanical stress along the skull is different for each skull-morphotype and depends directly on the shape of the skull. Consequently, each taxon with a different skull morphotype responding to different loadings in a given region might have a unique histological architecture of homologous bones.

Extent of remodelling. Among the sections from the *Metoposaurus* skull, four main degrees of remodeling could be observed in the middle region. Samples with the lowest degree of remodeling are from the postfrontal, parietal and supratemporal. A few large erosion cavities occur in the premaxilla, nasal, lacrimal, jugal, prefrontal, postparietal, squamosal, quadratojugal, and all studied bones from the palatal side of the skull. The maxilla is dominated by numerous, but moderately sized, erosion cavities. In the middle region of the tabular and squamosal 2, the

bone deposition exceeds the bone resorption and it does not represent the typical spongious structure.

The increase in remodeling extent is a known developmental character. Witzmann (2009) published the detailed histology of dermal bones from a young adult and adult *Mastodonsaurus,* and observed an increase in remodeling (expressed as an increase of the erosion cavities sizes) in the older specimen. In the *Metoposaurus*, different histological stages can be observed among different bones in one skull. The less remodeled (postfrontal, parietal and supratemporal) and highly remodeled (premaxilla, nasal, lacrimal, jugal, prefrontal, postparietal, squamosal, quadratojugal) bones seem to represent two stages of the same process, resulting in the increase in porosity of the middle region. This may indicate the sequence of the skull ossification during ontogeny, with the latest ossification of bones occurring on the central part of the skull roof. However, less remodeled samples originate from the grooves-ridges regions, whereas the other sections come from the reticulate areas. This confirms the hypothesis presented first by Bystrow (1935), that the polygonal reticulate structures are the center of ossification and that ridges-grooves areas show the direction and extent of growth from these ossification centers. In this case, different degrees of remodeling, which resemble the ontogenetic change, are the result of longitudinal growth of the bone.

Origin and dynamic of the sculpture pattern. Although dermal sculpture was early recognized as a characteristic of basal tetrapods (e.g. von Meyer, 1858; Fraas, 1889; Fritsch, 1889; Zittel, 1911), the morphogenesis of the sculptures is still an open question (summarized by Witzmann, 2009; Witzmann et al., 2010; de Buffrénil et al., 2016). Among extant tetrapods, growth of dermal bony tubercles and ridges has been studied in osteoderms of squamates and in dermal skull bones and osteoderms of crocodiles. In squamates, the presence of pits and ridges

316 on the external surface of osteoderms follows from both local resorption and growth of bone
317 (Zylberberg and Castanet, 1985; Levrat-Calviac & Zylberberg, 1986), whereas in crocodile
318 dermal bones, de Buffrénil (1982) and Cerda et al. (2015) stated that sculpture is mainly the
319 result of local resorption. In contrast, Vickaryous and Hall (2008) found no evidence for
320 morphogenesis of bone sculpture by resorption in *Alligator mississippiensis*, and presumed that
321 sculptural ridges develop by preferential bone growth. Concerning basal tetrapods, Bystrow
322 (1935, 1947) showed that the development of bone sculpture in the temnospondyls
323 *Benthosuchus*, *Platyoposaurus* and *Dvinosaurus* took place solely by growth of the bony ridges
324 and tubercles, and resorptive processes were not involved. The thin sections of the dermal bones
325 of skull and pectoral girdle in the basal tetrapods investigated by Witzmann (2009) corroborate
326 Bystrow's findings and show that the dermal sculpture did not develop by local resorption of the
327 bone surface, comparable to the pattern in basal tetrapod osteoderms (Witzmann & Soler-Gijón,
328 2008). According to the most recent study (de Buffrénil et al., 2016), the involvement of several
329 complex remodeling processes, with the local succession of resorption and reconstruction cycles,
330 is frequent and occurs in all major gnathostome clades, whereas the temnospondyl sections share
331 an important common feature: the lack of superficial remodeling (resorption and reconstruction
332 cycles). However, in the section of *Plagiosternum* described by Witzmann (2009), the eroded
333 external surface is illustrated. The supratemporal of *Metoposaurus krasiejowensis* (Fig. 5H)
334 confirms the observation of Witzmann (2009) and shows that the remodeling process might be
335 involved in the sculpture creation of Temnospondyli.

336 Moreover, the study of de Buffrénil et al. (2016) showed that, beside the resorption, other
337 dynamics processes also modify the sculpture during bone growth. Buffrénil et al. (2016)
338 observed six main patterns of such modification. The simplest one is repetition of the width or

339 position of pits and ridges from one growth stage to the following one. The ridges during the
340 bone deposition can drift symmetrically in two opposite directions, or the ridges around a given
341 pit may migrate in the same direction. Also, a change in size of the ridges is possible, resulting in
342 the gradual narrowing of pit diameter (convergent ridge drift), or opposite process may occur
343 when the reduction of ridge width is observed. In the most drastic case the pits can be entirely
344 filled and disappear to be replaced in situ by ridges.

345 In the skull bones of *Metoposaurus krasiejowensis*, newly deposited bone repeats the
346 pattern of sculptures in the younger stages (Fig. 5D-F). However, in the postfrontal, squamosal,
347 supratemporal, tabular, jugal, and quadratojugal, the alternation of valleys and ridges is
348 preserved (Fig. 5G). In this case the newly deposited ridges are created on the place of valleys,
349 but without resorption. The distance between newly created tops of the ridges is not distinctively
350 different from that in the previous generation.

351 Overall, the evidence indicates that the metric pattern of the sculpture is relatively stable,
352 but the position of the ridges and grooves is dynamic during growth as a specific adaptation to
353 different biomechanical loading on the new, larger bone.

354 **Skeletochronological information**. Long bones generally provide the best information
355 for bone skeletochronological studies (Castanet et al., 1993; Chinsamy-Turan, 2005; Erickson,
356 2005). This also applies in temnospondyls (Damiani, 2000; Steyer et al., 2004; Ray et al., 2009;
357 Mukherjee et al., 2010; Sanchez et al., 2010a; 2010b; Konietzko-Meier & Klein, 2013;
358 Konietzko-Meier & Sander, 2013; Konietzko-Meier & Schmitt, 2013; Sanchez & Schoch, 2013;
359 Konietzko-Meier et al., 2014). In the long bones, the three main types of growth marks are
360 known: fast growing zones, more slowly deposited annuli, and Lines of Arrested Growth (LAG-
361 s) that indicate the cessation of the growth (Francillon-Vieillot et al., 1990). Most often the full

annual growth cycle consists of a thick, fast growing zone, a thin, slow growing annulus, and one or more LAG-s. Moreover, in fast-growing amniotes, the several growth lines (LAG-s) present next to the surface of bone, known as the External Fundamental System (EFS) could be visible. An EFS indicates a slowing of growth, suggesting that the maximum size has been reached (Sander, 2000; Chinsamy-Turan, 2005; Erickson, 2005; Turvey et al., 2005; Sander et al., 2011). The dermal bones, e.g., osteoderms, have been used as well for skeletochronological analysis (Buffrénil & Buffetaut, 1981; Hutton, 1986; Hua & Buffrénil, 1996; Tucker, 1997; Scheyer & Sander, 2004; Hill & Lucas, 2006; Hayashi & Carpenter, 2007; Scheyer, 2007; Scheyer & Sánchez-Villagra, 2007; Hayashi et al., 2009; Klein et al., 2009). However, the results of these studies suggest that a careful use of osteoderms in skeletochronology of fossil specimens is required because of different growth patterns between the skeleton and osteoderms (Hayashi et al., 2009; Klein et al., 2009).

Even less is known about the preservation of growth marks in the temnospondyl dermal bones. Numerous growth marks in the external and internal cortices of the dermal bone have been observed in several temnospondyl taxa (Scheyer, 2007; Witzmann, 2009). However, without testing the whole growth series, it is not possible to estimate the amount of remodeled tissue and thus, no direct conclusion about the individual age of sectioned bones can be provided.

Histology of the long bones in *Metoposaurus krasiejowensis* is well known (Konietzko-Meier & Klein, 2013; Konietzko-Meier & Sander, 2013), and an evaluation and correlation of the growth patterns preserved in long bones and dermal bones is possible. Indirect estimation of the individual age of the studied skull is possible based on the morphological characters and size-comparison with the femora. Cranial sutures were not visible on the skull surface (Gruntmejer, 2012). The disappearance of all traces of sutures on the skull surface during ontogeny is a

phenomenon often encountered in adult individuals (Moazen et al., 2008). In the completely preserved skeletons of *Dutuitosaurus ouazzoui* (Dutuit, 1976), a skull of similar length (about 400 mm) to the one here described, corresponds with an approximately142 mm long femur (Dutuit, 1976: pl XXXI; personal observation DKM). Steyer et al. (2004) calculated the individual age of the adult *Dutuitosaurus* femur, comparable in length, as approximately eight or nine years. Comparing skeletochronological data of *Metoposaurus* with that of *Dutuitosaurus* revealed that the femora of overlapping sizes show a similar age in both taxa, and major developmental plasticity can be excluded (Konietzko-Meier & Klein, 2013). The individual age of the Krasiejów skull, based on comparison with *Dutuitosaurus,* can be thus estimated at about eight to ten years.

In the *Metoposaurus* skull, two types of growth alternation can be observed: numerous resting lines in the external cortex in the lacrimal, frontal, jugal, postfrontal, postparietal, tabular, and quadratojugal, and alternation of thick zones and annuli in the external cortex of the quadratojugal (Fig. 5F) and in the internal cortex of parasphenoid (Fig. 6G). In *Metoposaurus* long bones, such aggregations of resting lines are present not only in the outer part of the cortex but also deeper. It suggests that accumulation of external resting lines does not mean the cessation of growth at all (EFS), but only the oscillation in growth rate during one season (Konietzko-Meier & Klein, 2013; Konietzko-Meier & Sander, 2013). The complex with accumulation of resting lines is interpreted as a single annulus deposited during one, dry season (Konietzko-Meier & Sander, 2013; Konietzko-Meier & Klein, 2013) and together with the more vascularized zone represents a full annual growth cycle. However, in the skull, resting lines occur only once in the outermost part of external cortex following the high vascularized layer. Without a growth series it is not possible to state if the pattern known from long bones applies

also for dermal bones, and if older cycles have been already remodeled or if dermal bones show the independent growth outline. More informative are structures of the external cortex of the quadratojugal (Fig. 5F) and internal cortex in the parasphenoid (Fig. 6G), which resemble the growth sequence seen in *Metoposaurus* long bones (Konietzko-Meier & Klein, 2013; Konietzko-Meier & Sander, 2013). The two thick avascular layers represent the annuli, and combined with the two high vascularized zones indicate two growth seasons. Assuming that the age of the skull is about eight or nine years, with the preservation of two growth cycles, the number of remodeled growth marks could reach up to six to seven. This indicates a relatively fast remodeling rate of the dermal bones of the skull compared to the long bones and confirms that the dermal bones are not a good source of skeletochronological information.

Ossification processes of the skull. The quadrate and exoccipital show the periosteal ossification modus throughout the cartilage precursor. They consist of a trabecular middle region, surrounded by a thin layer of well-vascularized cortex. The preservation of cartilage (Fig. 7H), even during adulthood, indicates that ossification follows a pattern known for stereospondyl intercentra, with relatively slow ossification of the trabecular part and late development of the periosteal cortex (Konietzko-Meier et al., 2013; Konietzko-Meier et al., 2014).

The non-endochondral bones (dermal bones) may be formed through intramembranous ossification (dermal) or metaplastic ossification. Intramembranous ossification normally occurs in the deeper layers of connective tissue of the dermis of the skin (Francillon-Vieillot et al., 1990). Metaplastic bone develops via direct transformation of pre-existing, dense connective tissue, but in the absence of a periost, osteoblasts and osteoid (Vickaryous and Hall, 2008). Most often, the metaplastic and intramembranous domains occur together, creating many intermediate states between the intramebraneous bone, metaplastic bone, and even periosteal bone (Main et

al., 2005). The metaplastic component of the dermal bone represents interwoven structural fibers (Scheyer & Sander, 2004; Scheyer & Sánchez-Villagra, 2007). In the *Metoposaurus* skull, interwoven structural fibers are found as islets or larger areas in the external cortex in all bones from the skull roof. Moreover, in the postparietal investigated here, the ridges are composed completely of structural fibers. The common occurrence of ISF suggests that metaplastic ossification plays an important role during cranial development. In contrast, the fragments of *Metoposaurus* bone described by Witzmann (2009) have an external cortex that is solely composed of well-ordered parallel-fibered bone with no metaplastic tissue. The lack of IFS may indicate that those bones sectioned by Gross (1934) do not belong to skull.

Sharpey's fibers. In the long bones of *Metoposaurus*, the long Sharpey's fibers (SF1) indicate the remains of tendons and the shorter, very dense and evenly distributed fibers (SF2) are probably remains of bundles of collagenous fibers connecting periosteum to bone (Konietzko-Meier and Sander, 2013). In skull bones, also, both types of fibers could be recognized. In the prefrontal, frontal, postfrontal, parietal, supratemporal, squamosal, tabular and vomer, Sharpey's fibers are rare and occur mostly in the deeper parts of the sculptural ridges (Fig. 5C). In the premaxilla, maxilla, nasal, lacrimal, jugal, postorbital, postparietal, and quadratojugal, well-mineralized Sharpey's fibers are relatively short, but numerous, and sometimes packed densely in bundles. These fibers in cranial bone might represent tight anchorage of the dermis to the external bone surface, particularly to the sculptural ridges and tubercles, which served as the main points of anchorage for the skin.

The numerous long Sharpey's fibers packed in thick bundles are visible in the tabular. In this bone, the fibers occur also in the internal cortex. In the exoccipital, Sharpey's fibers are densely

454 packed in bundles, and they are much thicker and longer (Fig. 7D) than in the other bones. The
455 Sharpey's fibers occur here in similar amounts to those described in vertebrae (Konietzko-Meier
456 et al., 2013). Large concentrations of long, well mineralized Sharpey's fibers in the tabular and
457 exoccipital seem to be the obvious remains of strong muscle attachments and ligaments that
458 connect the skull to the vertebral column.
459
460 **Summary**
461 Among the bone of the *Metoposaurus krasiejowensis* skull, the variability is very high
462 and can be seen at both microanatomical and histological levels. The histological types are not
463 specifically bone-limited, but seem to be related to the specific area of the skull. The observed
464 pattern of remodeling progression suggests that the polygonal reticulate structures are the centers
465 of ossification and that ridges-grooves areas show the direction and extent of growth from these
466 ossification centers. The estimation of the individual age of the skull based on the morphological
467 characters and comparison with the femora suggests a relatively fast remodeling rate of the
468 dermal bones and confirms that the dermal bones are not a good source of skeletochronological
469 information. The dynamic processes present in the external cortex (resorption and the alternation
470 of the position of valleys and ridges) change the position of the ridges and grooves in what is a
471 specific adaptation to different biomechanical loading on the new, larger bone.
472 Three main types of ossification occur in the skull. The quadrate and exoccipital show a
473 periosteal ossification modus throughout the cartilage precursor. The preservation of cartilage,
474 even during adulthood, indicates that ossification follows a pattern known for stereospondyl
475 intercentra, with relatively slow ossification of the trabecular part and late development of the
476 periosteal cortex. The non-endochondral bones (dermal bones) may be formed through

intramembranous ossification (dermal) or metaplastic ossification. The common occurrence of ISF suggests that the metaplastic ossification plays an important role during the skull development. Short and dense Sharpey's fibers (SF2) visible in the external cortex are probably remains of tight anchorage of the dermis to the external bone surface. The numerous Sharpey's fibers packed in bundles, visible in the tabular and exoccipital, are the remains of strong muscle attachments and ligaments that connect the skull to the vertebral column.

ACKNOWLEDGEMENTS

The authors acknowledge Olaf Dülfer (University of Bonn, Steinman Institute) for preparing some of the thin-sections. We are grateful to Kayleigh Wiersma (University of Bonn, Steinmann Institute) for improving the English. Aurore Canoville and Martin Sander are acknowledged for fruitful discussion. We thank both reviewers (Torsten Scheyer and Ignacio Cerda) and the editor (Andrew Farke) for all comments which greatly improved our paper.

REFERENCES

1. Bodzioch A, Kowal-Linka M. 2012. Unraveling the origin of the Late Triassic multitaxic bone accumulation at Krasiejow (S Poland) by diagenetic analysis. *Palaeogeography, Palaeoclimatology, Palaeoecology* 346/347:25-36.
2. Brusatte SL, Butler RJ, Sulej T, Niedźwiedzki R. 2010. The taxonomy and anatomy of rauisuchian archosaurs from the Late Triassic of Germany and Poland. *Acta Palaeontologica Polonica* 54:221-230.

3. Brusatte SL, Butler MJ, Mateus O, Steyer JS. 2015. A new species of *Metoposaurus* from the Late Triassic of Portugal and comments on the systematics and biogeography of Metoposaurid temnospondyls. *Journal of Vertebrate Paleontology* 35(3):e912988.
4. Buffrénil de V. 1982. Morphogenesis of bone ornamentation in extant and extinct crocodilians. *Zoomorphology* 99(2):155-166.
5. Buffrénil de V, Buffetaut E. 1981. Skeletal growth lines in an Eocene crocodilian skull from Wyoming as an indicator of ontogenetic age and paleoclimatic conditions. *Journal of Vertebrate Paleontology* 1:57-66.
6. Buffrénil de V, Dauphin Y, Rage JC, Sire JY. 2011. An enamellike tissue, osteodermine, on the osteoderms of a fossil anguid (Glyptosaurinae) lizard. *Comptes Rendus Palevol* 10:427-437.
7. Buffrénil de V, Clarac F, Canoville A, Laurin M. 2016. Comparative data on the differentiation and growth of bone ornamentation in gnathostomes (Chordata: Vertebrata). *Journal of Morphology* 277(5):634-70.
8. Burns M, Vickaryous MK, Currie PJ. 2013. Histological variability in fossil and recent alligatoroid osteoderms: Systematic and functional implications. *Journal of Morphology* 274:676-686.
9. Bystrow AP, 1935. Morphologische Untersuchungen der deckknochen Schädels der Stegocephalen. *Acta Zoologica* 16:65-141.
10. Bystrow AP. 1947. Hydrophilous and zenophilous labyrinthodonts. *Acta Zoologica* 28:137-164.

11. Castanet J, Francillon-Vieillot H, Meunier FJ, Ricqlès de A. 1993. Bone and individual aging. In: Hall BK [ed] Bone. Volume 7: Bone Growth–B. CRC Press, Boca Raton, Florida. 245-283.

12. Castanet J, Francillon-Vieillot H, Ricqlès de A. 2003. The skeletal histology of the Amphibia. In: Heatwole H, Davies M [eds] Amphibian Biology, Volume 5, Osteology. Surrey Beatty and Sons, Chipping Norton, New South Wales, Australia. 1598-1683.

13. Cerda IA, Desojo JB, Trotteyn MJ, Scheyer TM. 2015. Osteoderm histology of Proterochampsia and Doswelliidae (Reptilia: Archosauriformes) and their evolutionary and paleobiological implications. *Journal of Morphology* 276(4):385-402.

14. Chinsamy-Turan A. 2005. The Microstructure of Dinosaur Bone: Deciphering Biology with Fine-scale Techniques. Johns Hopkins University Press, Baltimore. 1-195.

15. Chinsamy A, Raath MA. 1992. Preparation of fossil bone for histological examination. *Palaeontologia Africana* 29:39-44.

16. Clarac F, Souter T, Cornette R, Cubo J, Buffrénil de V. 2015. A quantitative assessment of bone area increase due to ornamentation in the Crocodylia. *Journal of Morphology* 276:1183-1192.

17. Clarac F, Souter T, Cubo J, Buffrénil de V, Brochu C, Cornette R. 2016. Does skull morphology constrain bone ornamentation? A morphometric analysis in the Crocodylia. *Journal of Anatomy* doi:10.1111/joa.12470.

18. Coldiron RW. 1974. Possible functions of ornament in labyrinthodont amphibians. *Occasional Papers of the Museum of Natural History of the University of Kansas*, *Lawrence* 33:1-19.

543 19. Damiani RJ. 2000. Bone histology of some Australian Triassic temnospondyl
544 amphibians: preliminary data. *Modern Geology* 24:109-124.
545 20. Dutuit JM. 1976. Introduction à l'etude paleontologique du Trias continental marocain.
546 Description des premiers Stegocephales recueillis dans le couloir d'Argana (Atlas
547 occidental). *Memoires du Museum National d'Histoire Naturelle Paris Ser. C* 36:1-253.
548 21. Dzik J. 2001. A new *Paleorhinus* fauna in the early Late Triassic of Poland. *Journal of*
549 *Vertebrate Paleontology* 21:625-627.
550 22. Dzik J. 2003. A beaked herbivorous archosaur with dinosaur affinities from the early Late
551 Triassic of Poland. *Journal of Vertebrate Paleontology* 23:556-574.
552 23. Dzik J. 2008. Gill structure and relationships of the Triassic cycloid crustaceans. *Journal*
553 *of Morphology* 269:1501-1519.
554 24. Dzik J, Sulej T. 2007. A review of the early Late Triassic Krasiejów biota from Silesia,
555 Poland. *Palaeontologia Polonica* 64:3-27.
556 25. Dzik J, Sulej T, Kaim A, Niedźwiedzki R. 2000. Późnotriasowe cmentarzysko
557 kręgowców lądowych w Krasiejowie na Śląsku Opolskim. *Przegląd Geologiczny* 48:226-
558 35.
559 26. Enlow DH, Brown SO. 1956. A comparative histological study of fossil and recent bone
560 tissues. *I. Texas Journal of Science* 8:405-43.
561 27. Erickson GM. 2005. Assessing dinosaur growth patterns: a microscopic revolution.
562 *Trends in Ecology and Evolution* 20(12):677-84.
563 28. Fortuny J, Marcé-Nogué J, de Esteban-Trivigno S, Gil L, Galobart Á. 2011.
564 Temnospondyli bite club: ecomorphological patterns of the most diverse group of early
565 tetrapods. *Journal of Evolutionary Biology* 24:2040-2054.

566 29. Fortuny J, Marce´-Nogue´ J, Gil L, Galobart Á. 2012. Skull mechanics and the
567 evolutionary patterns of the otic notch closure in Capitosaurs (Amphibia:
568 Temnospondyli). *The Anatomical Record* 295:1134-1146.
569 30. Fraas E. 1889. Die Labyrinthodonten der Schwäbischen Trias. *Palaeontographica* 36:1-
570 158.
571 31. Francillon-Vieillot H, de Buffrénil V, Castanet J, Géraudie J, Meunier FJ, Sire JY,
572 Zylberberg L, de Ricqlès A. 1990. Microstructure and mineralization of vertebrate
573 skeletal tissues. In: Carter JG [ed.]: Skeletal Biomineralization: Patterns, Processes and
574 Evolutionary Trends, Vol. I. Van Nostrand Reinhold, New York. 471-530.
575 32. Fritsch A. 1889. Fauna der Gaskohle und der Kalksteine der Permformation Böhmens,
576 Vol. 2. Prag: Selbstverlag. 1-132.
577 33. Gross W. 1934. Die Typen des mikroskopischen Knochenbaues bei fossilen
578 Stegocephalen und Reptilien. *Zeitschrift für Anatomie und Entwicklungsgeschichte*
579 203:731-64.
580 34. Gruntmejer K. 2012. Morphology and function of cranial sutures of the Triassic
581 amphibian *Metoposaurus diagnosticus* (Temnospondyli) from southwest Poland. In: Jagt-
582 Yazykova E, Jagt J, Bodzioch A, Konietzko-Meier D [eds] Krasiejów – palaeontological
583 inspirations. *ZPW Plik*, Bytom. 34-54.
584 35. Gruszka B, Zieliński T. 2008. Evidence for a very low-energy fluvial system: a case
585 study from the dinosaur-bearing Upper Triassic rocks of Southern Poland. *Geological*
586 *Quarterly* 52:239-252.

587 36. Hayashi S, Carpenter K. 2007. Different growth patterns between the body skeleton and
588 osteoderms of *Stegosaurus* (Ornithischia: Threophora). *Journal of Vertebrate*
589 *Paleontology* 27 (Suppl.): 88A.
590 37. Hayashi S, Carpenter C, Suzuki D. 2009. Different growth patterns between the skeleton
591 and osteoderms of *Stegosaurus* (Ornithischia, Thyreophora). *Journal of Vertebrate*
592 *Paleontology* 29:123-131.
593 38. Hill RV, Lucas SG. 2006. New data on the anatomy and relationships of the Paleocene
594 crocodylian Akanthosuchus langstoni. Acta Palaeontologica Polonica 51:455-464.
595 39. Hua S, Buffrénil de V. 1996. Bone histology as a clue in the interpretation of functional
596 adaptations in the Thalattosuchia (Reptilia, Crocodylia). *Journal of Vertebrate*
597 *Paleontology* 16:703-717.
598 40. Hutton JM. 1986. Age determination of living Nile crocodiles from the cortical
599 stratification of bone. *Copeia* 2:332-341.
600 41. Klein N, Scheyer T, Tütken T. 2009. Skeletochronology and isotopic analysis of a
601 captive individual of *Alligator mississippiensis* Daudin, 1802. *Fossil Record* 12(2):121-
602 131.
603 42. Konietzko-Meier D, Klein N. 2013. Unique growth pattern of *Metoposaurus diagnosticus*
604 *krasiejowensis* (Amphibia, Temnospondyli) from the Upper Triassic of Krasiejów,
605 Poland. *Palaeogeography Palaeoclimatology Palaeoecology* 370:145-157.
606 43. Konietzko-Meier D, Sander PM. 2013. Long bone histology of *Metoposaurus*
607 *diagnosticus* (Temnospondyli) from the Late Triassic of Krasiejów (Poland) and its
608 paleobiological implications. *Journal of Vertebrate Paleontology* 35(5):1-16.

609 44. Konietzko-Meier D, Schmitt A. 2013. Micro-CT-scan as a new, non-invasive method for
610 palaeohistological studies on the basis of a *Plagiosuchus* (Amphibia, Temnospondyli,
611 Plagiosauridae) femur. *The Netherlands Journal of Geosciences* 92(2/3):97-108.
612 45. Konietzko-Meier D, Bodzioch A, Sander PM. 2013. Histological characteristics of the
613 vertebral intercentra of *Metoposaurus diagnosticus* (Temnospondyli) from the Upper
614 Triassic of Krasiejów (Upper Silesia, Poland). *Earth and Environmental Science*
615 *Transactions of the Royal Society of Edinburgh* 103:1-14.
616 46. Konietzko-Meier D, Danto M, Gądek K. 2014. The microstructural variability of the
617 intercentra among temnospondyl amphibians. *Biological Journal of the Linnean Society*
618 112:747-764.
619 47. Levrat-Calviac V, Zylberberg L. 1986. The structure of the osteoderms in the gekko:
620 *Tarentola mauritanica*. *American Journal of Anatomy* 176:437-446.
621 48. Lucas SG. 2015. Age and correlation of Late Triassic tetrapods from southern Poland.
622 *Annales Societatis Geologorum Poloniae* 85(4):627-635.
623 49. Lucas SG, Spielmann JA, Hunt AP. 2007. Bio-chronological significance of Late Triassic
624 tetrapods from Krasiejów, Poland. *New Mexico Museum of Natural History and Science*
625 *Bulletin* 41:248-258.
626 50. Main RP, Ricqlès de A, Horner JR, Padian K. 2005. The evolution and function of
627 thyreophoran dinosaur scutes: implications for plate function in stegosaurs. *Paleobiology*
628 31:291-314.
629 51. Meyer H von. 1842. Labyrinthodonten—Genera. *Neues Jahrbuch für Mineralogie*,
630 *Geographie, Geologie, Palaeontologie* 1842:301-304.

631 52. Meyer H von. 1858. Reptilien aus der Steinkohlenformation in Deutschland.
632 *Palaeontographica* 6:59-219.
633 53. Moazen M, Curtis N, Evans SE, O'Higgins P, Fagan MJ. 2008. Rigid-body analysis of a
634 lizard skull: Modelling the skull of *Uromastyx hardwickii*. *Journal Biomechanics*
635 41:1274-1280.
636 54. Mukherjee D, Ray S, Sengupta DP. 2010. Preliminary observations of the bone
637 microstructure, growth patterns, and life habits of some Triassic Temnospondyls from
638 India. *Journal of Vertebrate Paleontology* 30(1):78-93.
639 55. Olempska E. 2004. Late Triassic spinicaudatan crustaceans from southwestern Poland.
640 *Acta Palaeontologica Polonica* 49(3):429-442.
641 56. Olempska E. 2011. Fresh-water ostracods from the Late Triassic of Poland. *Joannea*
642 *Geologie und Paläontologie* 11:154-155.
643 57. Racki G, Szulc J. 2014. Formacja grabowska – podstawowa jednostka litostratygraficzna
644 kajpru Górnego Śląska. *Przegląd Geologiczny* 63(2):103-113.
645 58. Ray S, Mukherjee D, Bandyopadhyay S. 2009. Growth patterns of fossil vertebrates as
646 deduced from bone microstructure: case studies from India. *Journal of Biosciences*
647 34:661-672.
648 59. Ricqlès de A. 1981. Recherches paléohistologiques sur les os longs des tétrapodes. VI.-
649 Stégocéphales. *Annales de Paléontologie* 67:141-160.
650 60. Rinehart LF, Lucas SG. 2013. The functional morphology of dermal bone ornamentation
651 in temnospondyl amphibian. In: Tanner LH, Spielmann JA, Lucas SG [eds] The Triassic
652 System. *New Mexico Museum of Natural History and Science, Bulletin* 61:524-532.

653 61. Sanchez S., Ricqlès de A, Schoch RR, Steyer JS. 2010a. Developmental plasticity of limb
654 bone microstructural organization in *Apateon*: histological evidence of paedomorphic
655 conditions in branchiosaurs. *Evolution & Development* 12:315-328.
656 62. Sanchez S, Schoch RR, Ricqlès de A, Steyer JS. 2010b. Palaeoecological and
657 palaeoenvironmental influences revealed by longbone palaeohistology: the example of
658 the Permian branchiosaurid *Apateon*. In : Vecoli M, Meyer CG [eds] The
659 Terrestrialization Process: Modeling Complex Interactions at the Biosphere-Geosphere
660 Interface. The Geological Society, London. 139-149.
661 63. Sanchez S, Schoch RR. 2013. Bone histology reveals a high environmental and metabolic
662 plasticity as a successful evolutionary strategy in a long-lived homeostatic Triassic
663 Temnospondyl. *Evolutionary biology* 40(4):627-647.
664 64. Sander PM. 2000. Long bone histology of the Tendaguru sauropods: implications for
665 growth and biology. *Paleobiology* 26:466-488.
666 65. Sander PM, Klein N, Stein K, Wings O. 2011. Sauropod bone histology and its
667 implications for sauropod biology. In: Klein N, Remes K, Gee CT, Sander PM [eds]
668 Biology of the Sauropod Dinosaurs: Understanding the Life of Giants. Life of the Past
669 (series ed. J. Farlow). Indiana University Press, Bloomington. 276-302.
670 66. Scheyer TM. 2007. Skeletal histology of the dermal armor of Placodontia: the occurrence
671 of ‘postcranial fibro-cartilaginous bone’ and its developmental implications. *Journal of*
672 *Anatomy* 211:737-753.
673 67. Scheyer TM, Sander PM. 2004. Histology of ankylosaur osteoderms: implications for
674 systematics and function. *Journal of Vertebrate Paleontology* 24:874-893.

675 68. Scheyer TM, Sánchez-Villagra MR. 2007. Carapace bone histology in the giant
676 pleurodiran turtle *Stupendemys geographicus*: phylogeny and function. *Acta*
677 *Palaeontologica Polonica* 52:137-154.
678 69. Scheyer TM, Desojo JB, Cerda IA. 2014. Bone histology of phytosaur, aetosaur, and
679 other archosauriform osteoderms (Eureptilia, Archosauromorpha). *Anatomical Record*
680 297:240-260
681 70. Schoch RR. 1999. Comparative osteology of *Mastodonsaurus giganteus* (Jaeger, 1828)
682 from the Middle Triassic (Lettenkeuper: Longobardian) of Germany (Baden-
683 Württemberg, Bayern, Thüringen). *Stuttgarter Beiträge zur Naturkunde Serie B*
684 *(Geologie und Paläontologie)* 278:1-170.
685 71. Schoch RR, Milner AR. 2000. Stereospondyli. *Handbuch der Palaeoherpetologie* 3B.
686 Munich: Verlag Dr. Friedrich Pfeil 1-230.
687 72. Skawina A. 2013. Population dynamics and taphonomy of the Late Triassic (Carnian)
688 freshwater bivalves from Krasiejów (Poland). Palaeogeography, Palaeoclimatology,
689 Palaeoecology 379:68-80.
690 73. Skawina A, Dzik J. 2011. Umbonal musculature and relationships of the Late Triassic
691 filibranch unionoid bivalves. *Zoological Journal of the Linnean Society* 163:863-883.
692 74. Skrzycki P. 2015. New species of lungfish (Sarcopterygii, Dipnoi) from the Late Triassic
693 Krasiejów site in Poland, with remarks on the ontogeny of Triassic dipnoan tooth plates.
694 *Journal of Vertebrate Paleontology* 35(5):e964357.
695 75. Steyer JS, Laurin M, Castanet J, Ricqlès de A. 2004. First histological and
696 skeletochronological data on temnospondyl growth: palaeoecological and

palaeoclimatological implications. *Palaeogeography, Palaeoclimatology, Palaeoecology* 206:193-201.

76. Sulej T. 2002. Species discrimination of the Late Triassic temnospondyl amphibian Metoposaurus diagnosticus. *Acta Paleontologia Polonica* 47(3):535-546.
77. Sulej T. 2005. A new rauisuchian reptile (Diapsida: Archosauria) from the Late Triassic of Poland. *Journal of Vertebrate Paleontology* 25(1):78-86.
78. Sulej T. 2007. Osteology, variability, and evolution of *Metoposaurus*, a temnospondyl from the Late Triassic of Poland. *Paleontologia Polonica* 64:29-139.
79. Sulej T. 2010. The skull of an early Late Triassic aetosaur and the evolution of the stagonolepidid archosaurian reptiles. *Zoological Journal of the Linnean Society* 158:860-881.
80. Sulej T. Majer D. 2005. The temnospondyl amphibian *Cyclotosaurus* from the Upper Triassic of Poland. *Palaeontology* 48:157-170.
81. Szulc J, Racki G, Jewuła K. 2015a. Key aspects of the stratigraphy of the Upper Silesian middle Keuper, southern Poland. *Annales Societatis Geologorum Poloniae* 85(4):557-586.
82. Szulc J, Racki G, Jewuła K, Środoń J. 2015b. How many Upper Triassic bone–bearing levels are there in Upper Silesia (southern Poland)? A critical overview of stratigraphy and facies. *Annales Societatis Geologorum Poloniae* 85(4):587-626.
83. Tucker A D. 1997. Validation of skeletochronology to determine age of freshwater crocodiles (*Crocodylus johnstoni*). *Marine &Freshwater Research* 48:343-351.
84. Turvey SP, Green OR, Holdaway RN. 2005. Cortical growth marks reveal extended juvenile development in New Zealand moa. *Nature* 435:940-943.

720 85. Vickaryous MK, Hall BK. 2008. Development of the dermal skeleton in *Alligator*
721 *mississippiensis* (Archosauria, Crocodylia) with comments on the homology of
722 osteoderms. *Journal of Morphology* 269:398-422.
723 86. Vickaryous MK, Sire JY. 2009. The integumentary skeleton of tetrapods: origin,
724 evolution, and development. *Journal of Anatomy* 214:441-464.
725 87. Witzmann F. 2009. Comparative histology of sculptured dermal bones in basal tetrapods,
726 and the implications for the soft tissue dermis. *Palaeodiversity* 2:233-270.
727 88. Witzmann F, Soler-Gijón R. 2008. The bone histology of osteoderms in temnospondyl
728 amphibians and in the chroniosuchian *Bystrowiella*. *Acta Zoologica* (Stockholm) 91: 96-
729 114.
730 89. Witzmann F, Scholz H, Müller J, Kardjilov N. 2010. Sculpture and vascularization of
731 dermal bones, and the implications for the physiology of basal tetrapods. *Zoological*
732 *Journal of the Linnean Society* 160:302-340.
733 90. Zittel KA. 1911. Grundzüge der Paläontologie (Paläozoologie). II. Abteilung. Vertebrata.
734 Verlag von R. Oldenbourg, München and Berlin. 1-589.
735 91. Zylberberg L, Castanet J. 1985. New data on the structure and the growth of the
736 osteoderms in the reptile *Anguis fragilis* L. (Anguidae, Squamata). *Journal of*
737 *Morphology* 186:327-342.
738
739
740
741
742

743

744 **Fig. 1.** The skull of *Metoposaurus krasiejowensis* (UOPB 01029) from the Late Triassic of
745 Poland. **(A)** Dorsal view of skull; **(B)** Ventral view of the skull. Scale bar equals 10 cm.

746

747 **Fig. 2.** The sectioning planes of the *Metoposaurus krasiejowensis* skull (UOPB 01029) from the
748 Late Triassic of Poland. **(A)** The skull roof; **(B)** The palatal side of the skull. The sectioning
749 planes are marked by red lines. Grey color indicates preserved parts of the skull; the destroyed or
750 sediment-covered regions are indicated by the light yellow color. Scale bar equals 10 cm.
751 Abbreviations ex = exoccipital, f = frontal, j = jugal, l = lacrimal, m = maxilla, n = nasal, p =
752 parietal, pf = postfrontal, pm = premaxilla, po = postorbital, pp = postparietal, prf = prefrontal, ps
753 = parasphenoid, pt = pterygoid, q = quadrate bone, qj = quadratojugal, sq1 = squamosal 1, sq2 =
754 squamosal 2, st = supratemporal, t = tabular, v = vomer.

755

756 **Fig. 3.** General microanatomy of the skull bones of *Metoposaurus krasiejowensis* (UOPB 01029)
757 from the Late Triassic of Poland. **(A)** premaxilla; **(B)** maxilla; **(C)** nasal; **(D)** lacrimal; **(E)**
758 prefrontal; **(F)** jugal/ postorbital; **(G)** postfrontal; **(H)** frontal; **(I)** parietal; **(J)** supratemporal; **(K)**
759 squamosal 1; **(L)** squamosal 2; **(M)** postparietal; **(N)** tabular; **(O)** quadratojugal; **(P)**
760 parasphenoid; **(Q)** vomer; **(R)** pterygoid; **(S)** quadrate bone; **(T)** exoccipital. Scale bar equals 10
761 mm. Abbreviations: ap = alary process, ds = dental shelf, vp = vomeral process.

762

763 **Fig. 4.** Detailed microanatomy of the skull bones of *Metoposaurus krasiejowensis (*UOPB
764 01029) from the Late Triassic of Poland, based on the frontal. **(A)** A valley and two ridges; **(B)**
765 Enlargement of (A); the external and internal cortex, and trabecular middle region with

numerous and large erosion cavities are visible; image in cross-polarized light; **(C)** The same as (B), but in plane-polarized light. Dashed lines mark the approximate border between the external cortex/middle region/internal cortex. Scale bars equal 10 mm for (A), and 500 μm for (B-C). Abbreviations: EC = external cortex, ER = erosion cavities, IC = internal cortex, LB = lamellar bone, MR = middle region, PFB = parallel-fibered bone, r = rigde, v = valley.

Fig. 5. Histology of the external cortex of the skull bones of *Metoposaurus krasiejowensis* (UOPB 01029) from the Late Triassic of Poland. **(A)** Magnification of external cortex of the frontal; **(B)** Same as (A), but in cross-polarized light; **(C)** External cortex of the tabular with distinct Sharpey's fibers in the area of the sculptural ridges; **(D)** A succession of longitudinally and transversely cut ISF parts; **(E)** The resting lines (black arrows) in the cortex of squamosal 2; **(F)** Zones and annuli present in the external cortex of the quadratojugal; **(G)** Alternation of valleys and ridges in the postfrontal; note that remains of lamellar bone in the deep part of cortex are present, representing the bottom of a valley from an older generation; **(H)** The cementing lines (white arrows) visible in the superficial part of external cortex the supratemporal. Dashed lines mark the approximate border between the external cortex/middle region/internal cortex. Images (A), (E) and (H) in plane-polarized light, others in cross-polarized light. Scale bars equal for (A-E) and (H) 100 μm and for (F)-(G) 500 μm. Abbreviations: A = annulus; FLB = fibro-lamellar bone; L-ISF = longitudinally cut Interwoven Structural Fibers; OL = osteocyte lacunae, PO = primary osteons, r = ridge, SF = Sharpey's fibers, T-ISF = transversely cut Interwoven Structural Fibers, v = valley, Z = zone.

788 **Fig. 6.** Details of the histology of the middle region and internal cortex of the skull (UOPB
789 01029) bones of *Metoposaurus krasiejowensis* from Late Triassic of Poland. **(A)** Large erosion
790 cavities present in the middle region of the vomer; **(B)** Poorly remodeled, well vascularized
791 middle region of the parietal; **(C)** Poorly vascularized fragment of the squamosal 2; **(D)** Nearly
792 avascular internal cortex with resting lines (black arrows) visible in the parietal; **(E)** Internal
793 cortex of the premaxilla, note the relatively numerous vascular canals; **(F)** Internal cortex of the
794 jugal with very numerous vascular, small vascular canals; **(G)** Alternation of thick annuli and
795 zones visible in the internal cortex of the parasphenoid. Dashed lines mark the approximately
796 border between the external cortex/middle region/internal cortex. Image (G) in cross-polarized
797 light, others in plane-polarized light. Scale bars equal 100 μm for (D) and (G) and 500 μm for
798 other photographs. Abbreviations: A = annulus, EC = external cortex, IC = internal cortex, MR =
799 middle region, SO = secondary osteon, VC = vascular canals, Z = zone.
800
801 **Fig. 7.** Histological details of the quadrate (A-C) and exoccipital (D-H) of *Metoposaurus*
802 *krasiejowensis* skull (UOPB 01029) from Late Triassic of Poland. **(A)** Fragment of cortex of the
803 quadrate; **(B)** The same as (A), but in cross-polarized light; **(C)** Trabecular bone of the quadrate
804 bone; **(D)** Fragment of cortex of the exoccipital with distinct Sharpey's fibers; **(E)** Close-up of
805 (D), note that the Sharpey's fibers are also visible in plane-polarized light; **(F)** The same as (E)
806 but in cross-polarized light. Both images (E) and (F) are rotated clockwise for better arrangement
807 of the figures; **(G)** Trabeculae visible in the central part of the exoccipital; **(H)** Remains of
808 calcified cartilage preserved in the trabeculae part of exoccipital. Images (A), (C), (E), and (G) in
809 plane-polarized light, others in cross-polarized light. Scale bars equal 500 μm for (C), (D) and
810 (G), and 100 μm for other photographs. Abbreviations: C = cortex, CC = calcified cartilage, ER

811 = erosion cavities, LB = lamellar bone, OL = osteocyte lacunae, PO = primary osteons, PFL =
812 parallel-fibered bone, SO = secondary osteons, SF = Sharpey's fibers, TR = trabecular region,
813 VC = vascular canals.
814

Table 1(on next page)

Microanatomy of the sampled bones of *Metoposaurus krasiejowensis* skull (UOPB 01029).

[1]The average thickness of entire bone was estimated in thin sections, expressed as an arithmetical average from three measurements of the thickness of a bone taken on the bottom of valleys and the top of ridges[, 2] For the estimation of ratio between external cortex (E), medial region (M) and internal cortex (I): E:M:I, the thickness of external cortex was taken as one and then proportionally the value for medial region and internal cortex were calculated; *Non-dermal bone.

1 Microanatomy of the sampled bones of *Metoposaurus krasiejowensis* skull (UOPB 01029).

bone	ornamentation	min-max thickness (µm)	average thickness (µm)[1]	E:M:I[2]	thickness of the external cortex (µm)
premaxilla -allary process (pm)	not preserved	3000 - 6000	4081.2	1:1.1:0.9	1331,0
maxilla (m) - dorsal process	not preserved	~3500-4500	~3060,0	1:1.1:0.9	~1020.0
nasal (n)	relatively high ridges (about 1000 µm)	4500-7000	4758.0	1:1.2:0.4	1830.0
lacrimal (l)	medium high (500 µm), steep ridges and wide grooves	4500-6500	5940.0	1:1.6:0.7	1800.0
prefrontal (prf)	medium high (500 µm) and steep ridges	3900-5000	4256.0	1:1.7:0.8	1150.0
jugal (j)	high ridges (about 1000 µm) and wide grooves	5000-8000	6940.0	1:1.5:0.7	1800.0
postorbital (po)	high ridges (about 1000 µm) and wide grooves	5000-8000	6940.0	1:1.5:0.7	1800.0
postfrontal (pf)	low ridges (about 300 µm) and shallow grooves	3500-5000	3960.0	1:1.7:0.6	1200.0
frontal (f)	high ridges (about 1000 µm) and wide grooves	4000-6000	5549.0	1:1.5:0.6	1790.0
parietal (p)	high ridges (about 1000 µm) and narrow pits	3100-4500	3840.0	1:1.6:0.6	1200.0
supratemporal (st)	high ridges (about 1500 µm) and wide grooves	2000-6500	4800.0	1:1.6:0.6	1500.0
squamosal 1 (sq1)	very high ridges (up to 2000 µm) and wide grooves	3000-5000	3915.0	1:1.2:0.7	1350.0
squamosal 2 (sq2)	high ridges (about 1000 µm) and wide grooves	1500-5000	2250.0	1:0.3:0.5	1250.0
postparietal	steep, high ridges	7000-10000	8670.0	1:1.9:0.5	2550.0

(pp)	(about 1500 μm) and polygonal pits				
tabular (t)	high ridges (about 1000 μm) and wide pits	7000-11000	10000.0	1:2.2:0.8	2500.0
quadratojugal (qj)	high ridges (about 1000 μm) and wide grooves	4000-6000	5610.0	1:1.7:0.6	1700.0
vomer (v)	no clear sculpture	2000-5000	2925.0	1:2.8:0.7	650.0
parasphenoid (ps)	no clear sculpture	2000-4700	4050.0	1:2:1.5	900.0
pterygoid (pt)	no clear sculpture	4500-7000	5460.0	1:5.4:2	650.0
quadrate bone (q)*	-	diameter 20000 μm			
exoccipital (ex)*	-	diameter 20000 μm			

[1]The average thickness of entire bone was estimated in thin sections, expressed as an arithmetical average from three measurements of the thickness of a bone taken on the bottom of valleys and the top of ridges; [2] For the estimation of ratio between external cortex (E), medial region (M) and internal cortex (I): E:M:I, the thickness of external cortex was taken as one and then proportionally the value for medial region and internal cortex were calculated;

*Non-dermal bone

Figure 1(on next page)

The skull of Metoposaurus krasiejowensis [i](UOPB 01029) from the Late Triassic of Poland.

(A) **Dorsal view of skull; (B)** Ventral view of the skull. Scale bar equals 10 cm.

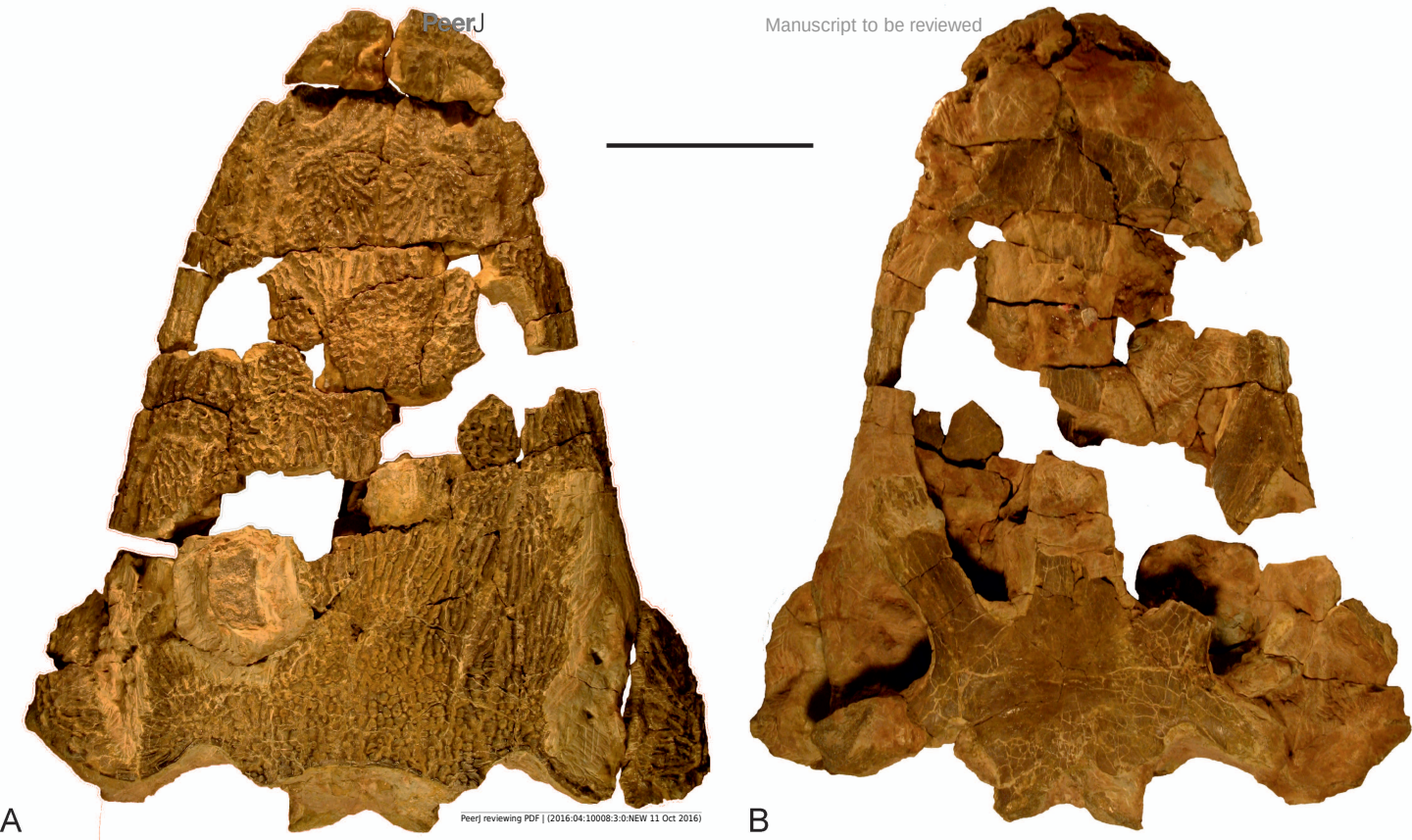

Figure 2(on next page)

The sectioning planes of the Metoposaurus krasiejowensis[i] skull (UOPB 01029) from the Late Triassic of Poland.

(A) **The skull roof; (B)** The palatal side of the skull. [b]The sectioning planes are marked by red lines. Dark grey color indicates preserved parts of the skull; the destroyed or sediment-covered regions are indicated by the light grey color. Scale bar equals 10 cm. Abbreviations: pm = premaxilla, m = maxilla, n = nasal, l = lacrimal, prf = prefrontal, j = jugal, po = postorbital, pf = postfrontal, f = frontal, p = parietal, st = supratemporal, sq1 = squamosum 1, sq2 = squamosum 2, pp = postparietal, t = tabular, qj = quadratojugal, v = vomer, ps = parasphenoid, pt = pterygoid, q = quadrate bone, ex = exoccipital.

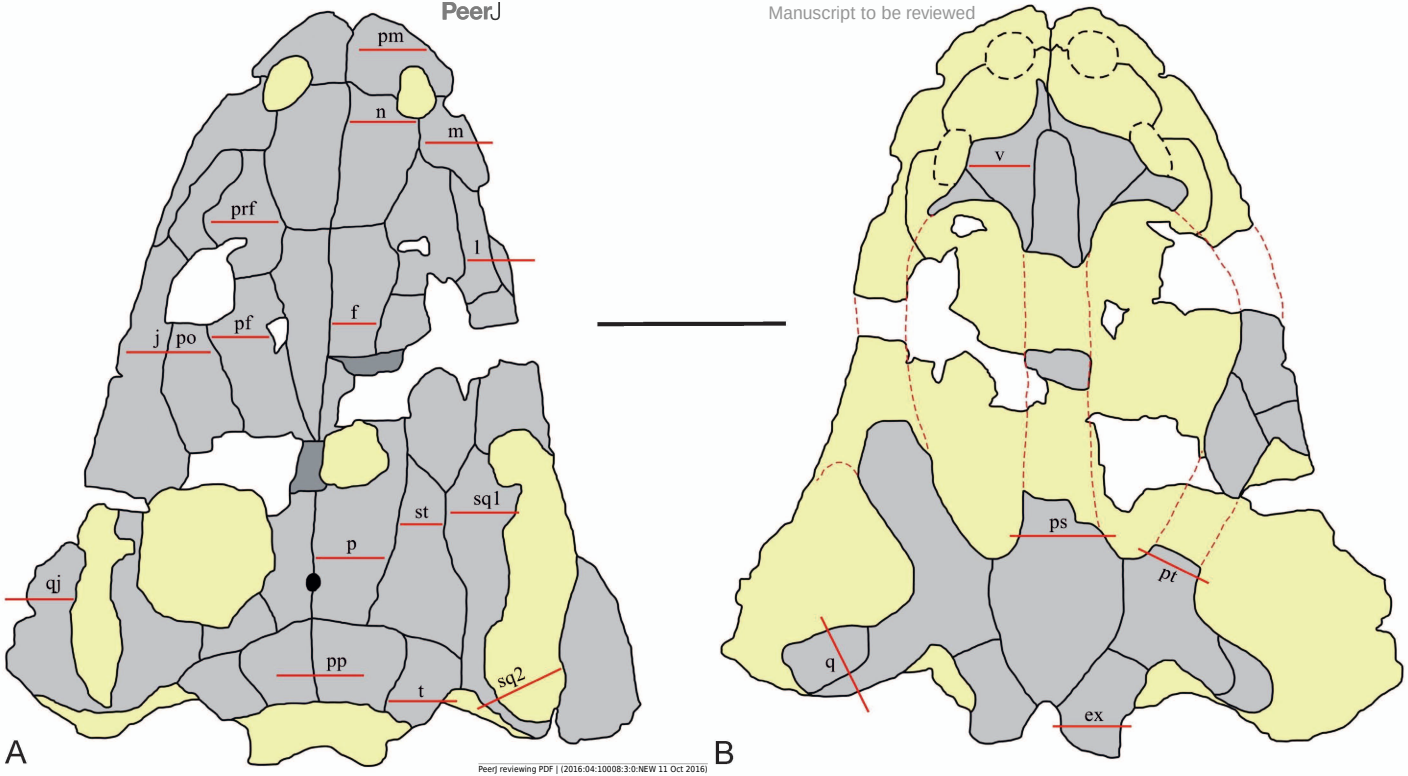
pm
n
m
prf
l
f
j
po
pf
st
sq1
p
qj
pp
t
sq2
A
v
ps
pt
q
ex
B

Figure 3(on next page)

General microanatomy of the skull bones of *Metoposaurus krasiejowensis* (UOPB 01029) from the Late Triassic of Poland.

(A) premaxilla; **(B)** maxilla; **(C)** nasal; **(D)** lacrimal; **(E)** prefrontal; **(F)** jugal/ postorbital; **(G)** postfrontal; **(H)** frontal; **(I)** parietal; **(J)** supratemporal; **(K)** squamosal 1; **(L)** squamosal 2; **(M)** postparietal; **(N)** tabular; **(O)** quadratojugal; **(P)** parasphenoid; **(Q)** vomer; **(R)** pterygoid; **(S)** quadrate bone; **(T)** exoccipital. Scale bar equals 10 mm. Abbreviations: ap = alary process, ds = dental shelf, vp = vomeral process.

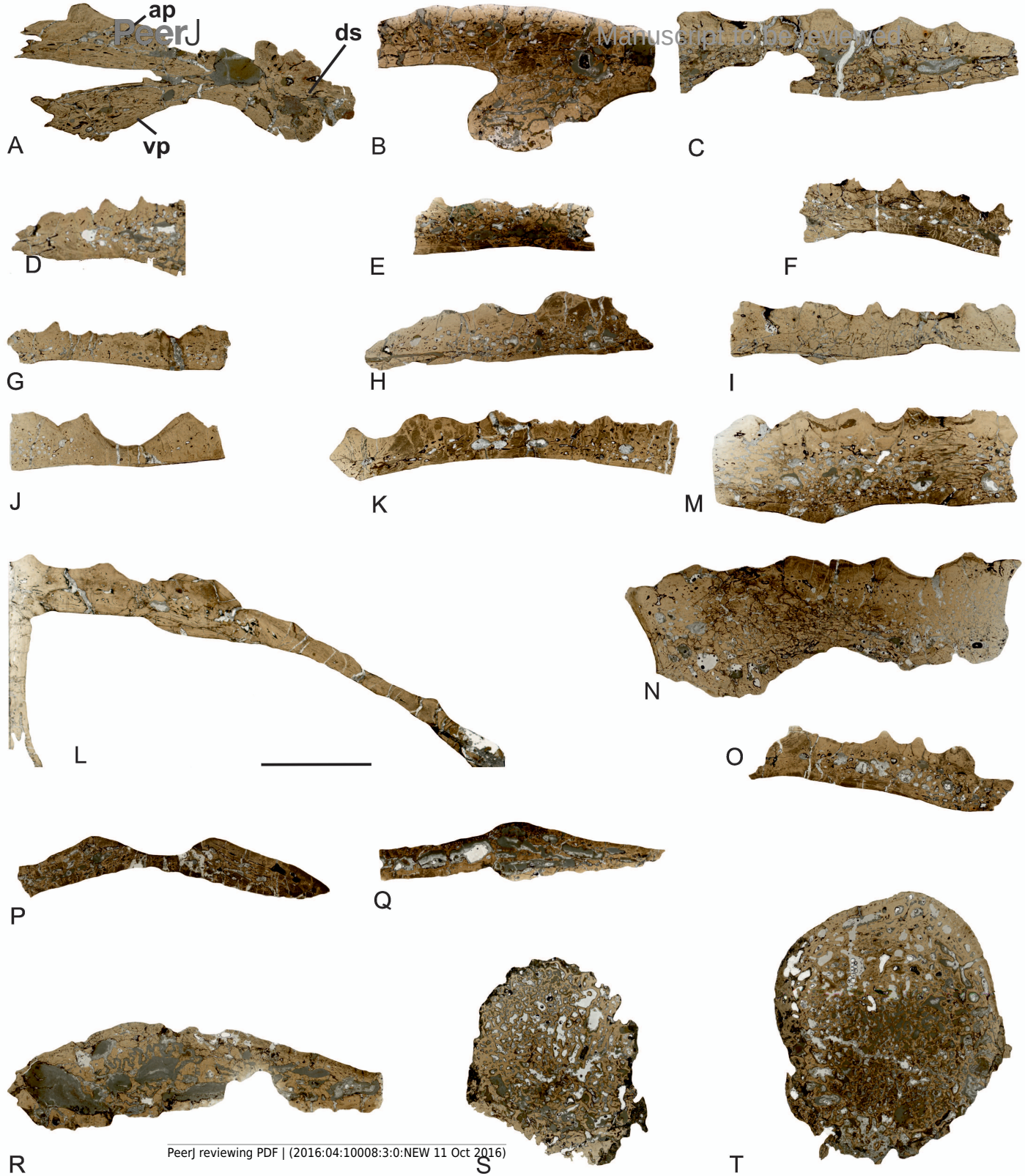

Figure 4(on next page)

Detailed microanatomy of the skull bones of *Metoposaurus krasiejowensis (*UOPB 01029) from the Late Triassic of Poland, based on the frontal.

(A) A valley and two ridges; **(B)** Enlargement of (A); the external and internal cortex, and trabecular middle region with numerous and large erosion cavities are visible; image in cross-polarized light; **(C)** The same as (B), but in plane-polarized light. Dashed lines mark the approximately border between the external cortex/middle region/internal cortex. Scale bars equal 10 mm for (A), and 500 µm for (B-C). Abbreviations: EC = external cortex, ER = erosion cavities, IC = internal cortex, LB = lamellar bone, MR = middle region, PFB = parallel-fibered bone, r = rigde, v = valley.

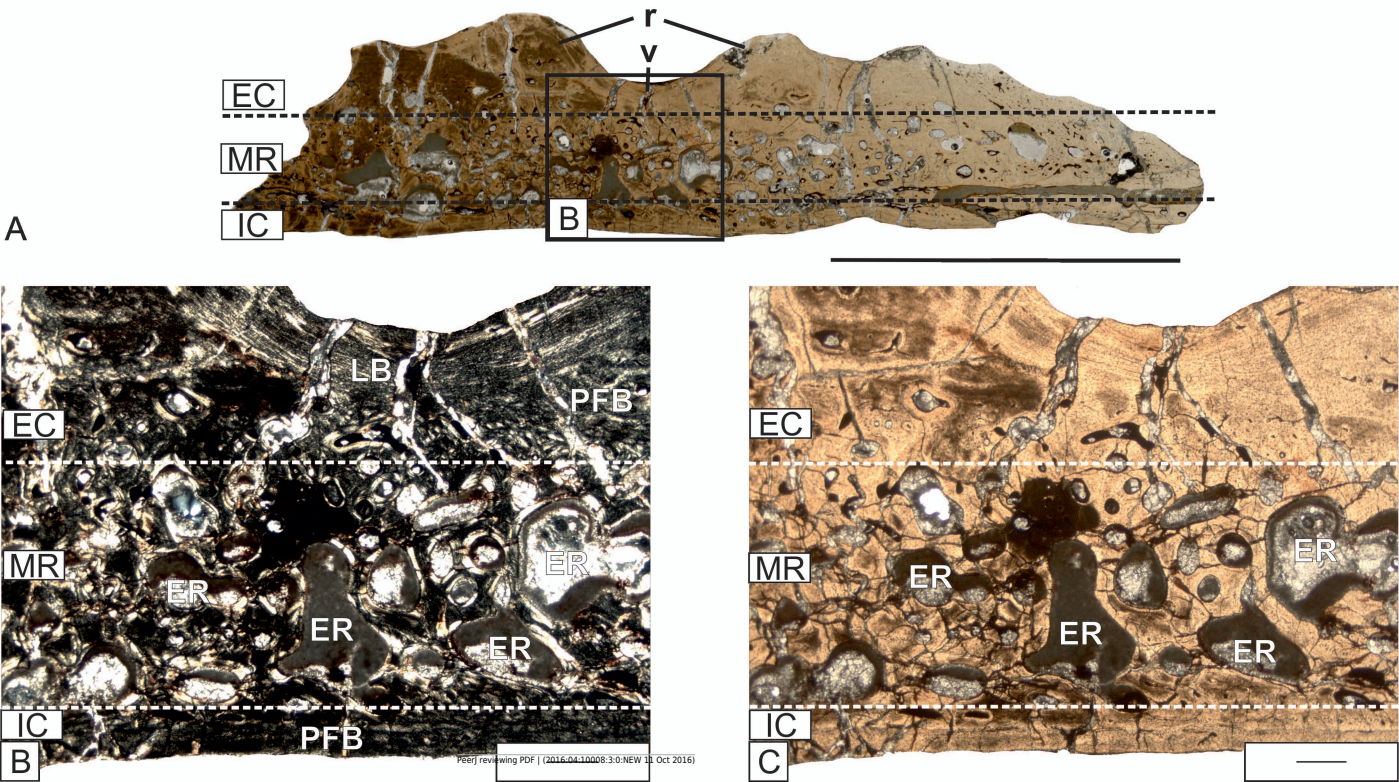
A
r
v
EC
MR
IC
B
LB
PFB
ER
ER
ER
ER
ER
PFB
B
EC
MR
ER
ER
ER
ER
ER
IC
C

Figure 5(on next page)

Histology of the external cortex of the skull bones of *Metoposaurus krasiejowensis* (UOPB 01029) from the Late Triassic of Poland.

(A) Magnification of external cortex of the frontal; **(B)** Same as (A), but in cross-polarized light; **(C)** External cortex of the tabular with distinct Sharpey's fibers in the area of the sculptural ridges; **(D)** A succession of longitudinally and transversely cut ISF parts; **(E)** The resting lines (black arrows) in the cortex of squamosal 2; **(F)** Zones and annuli present in the external cortex of the quadratojugal; **(G)** Alternation of valleys and ridges in the postfrontal, note that remains of lamellar bone in the deep part of cortex are present, representing the bottom of a valley from an older generation; **(H)** The cementing lines (white arrows) visible in the superficial part of external cortex the supratemporal. Dashed lines mark the approximate border between the external cortex/middle region/internal cortex. Images (A), (E) and (H) in plane-polarized light, others in cross-polarized light. Scale bars equal for (A-E) and (H) 100 µm and for (F)-(G) 500 µm. Abbreviations: A = annulus; FLB = fibro-lamellar bone; L-ISF = longitudinally cut Interwoven Structural Fibers; OL = osteocyte lacunae, PO = primary osteons, r = ridge, SF = Sharpey's fibers, T-ISF = transversely cut Interwoven Structural Fibers, v = valley, Z = zone.

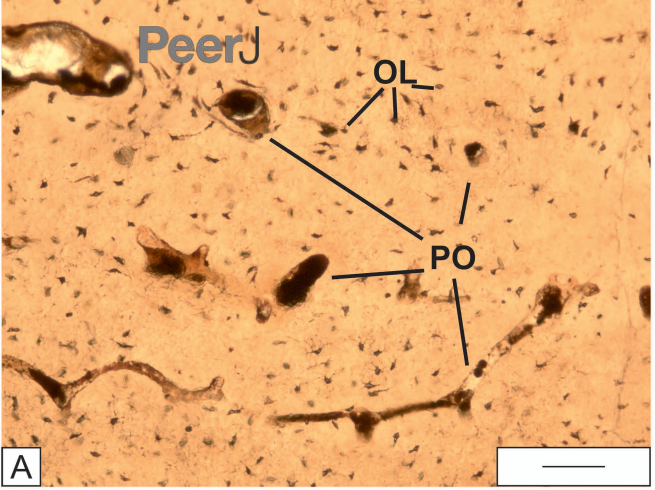

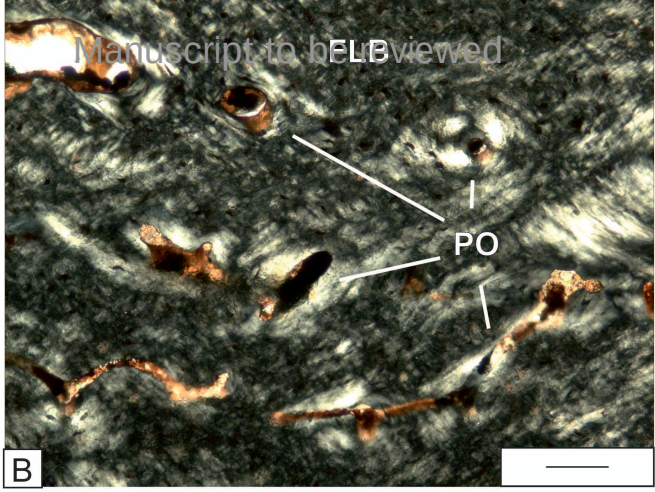

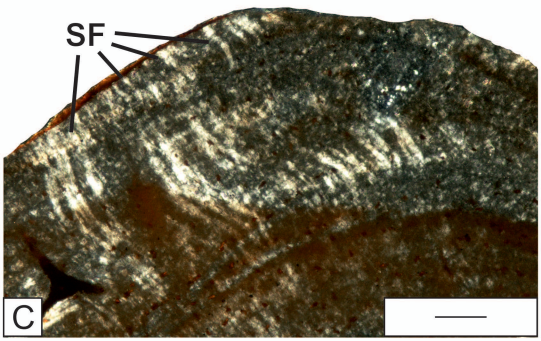

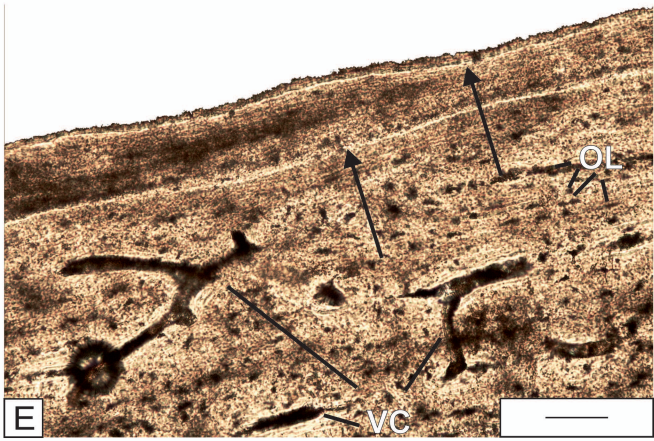

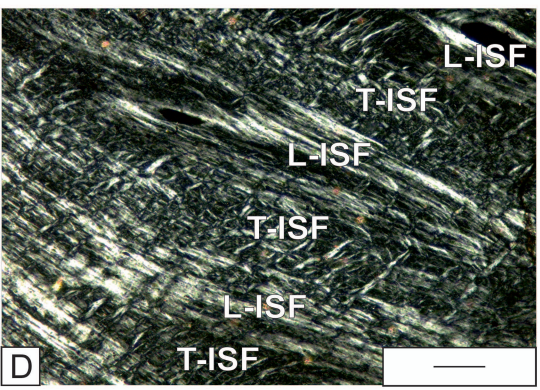

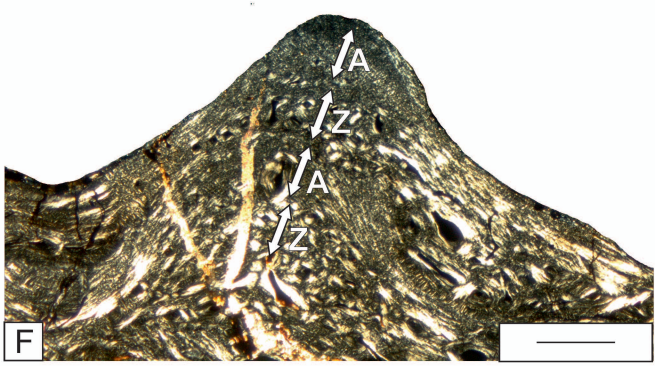

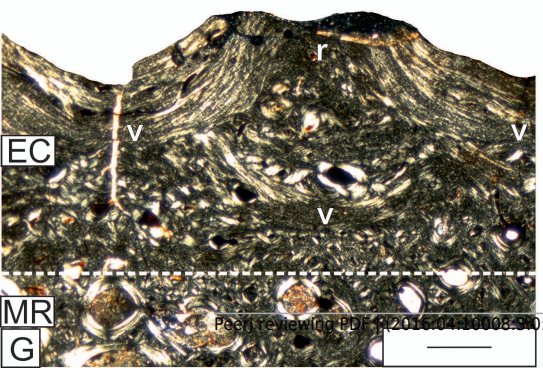

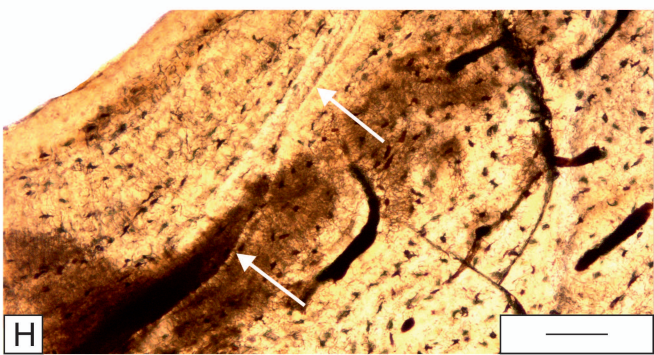

Figure 6(on next page)

The details of the histology of the middle region and internal cortex of the skull (UOPB 01029) bones of *Metoposaurus krasiejowensis* from the Late Triassic of Poland.

(A) Large erosion cavities present in the middle region of the vomer; **(B)** Poorly remodeled, well vascularized middle region of the parietal; **(C)** Poorly vascularized fragment of the squamosal 2; **(D)** Almost avascular internal cortex with resting lines (black arrows) visible in the parietal; **(E)** Internal cortex of the premaxilla, note the relatively numerous vascular canals; **(F)** Internal cortex of the jugal with very numerous vascular, small vscular canals; **(G)** Alternation of thick annuli and zones visible in the internal cortex of the parasphenoid. Dashed lines mark the approximately border between the external cortex/middle region/internal cortex. Image (G) in cross-polarized light, others in plane-polarized light. Scale bars equal 100 µm for (D) and (G) and 500 µm for other photographs. Abbreviations: A = annulus, EC = external cortex, IC = internal cortex, MR = middle region, SO = secondary osteon, VC = vascular canals, Z = zone.

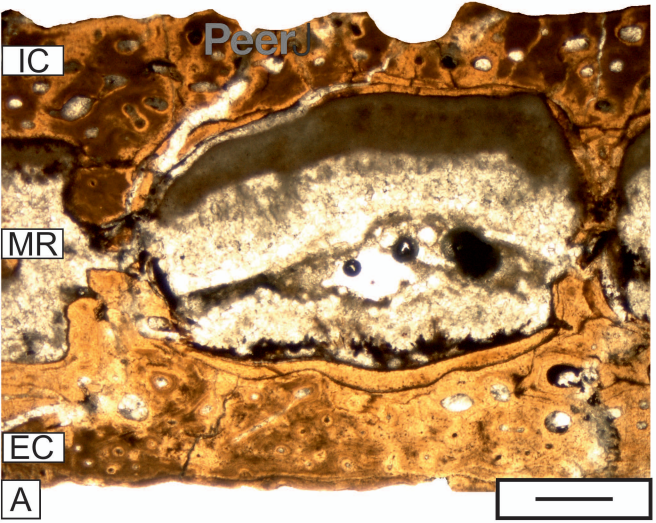

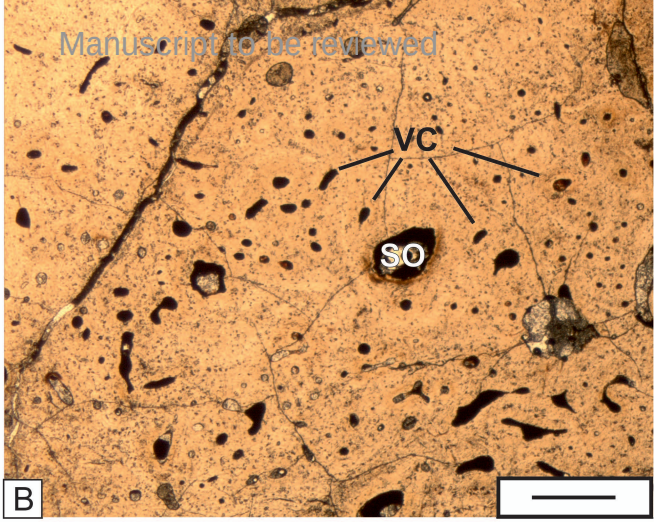

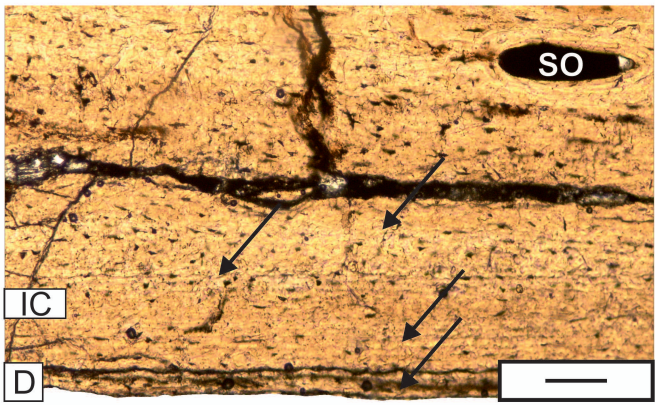

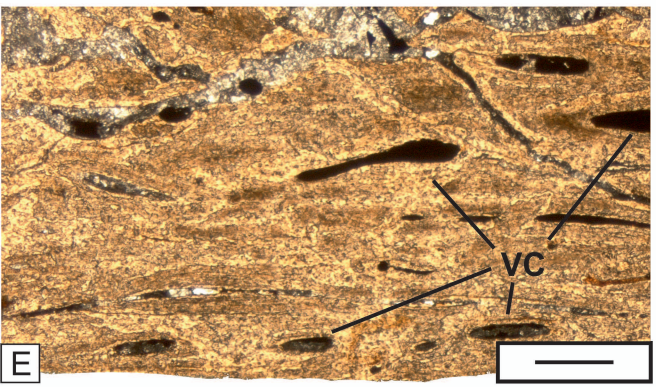

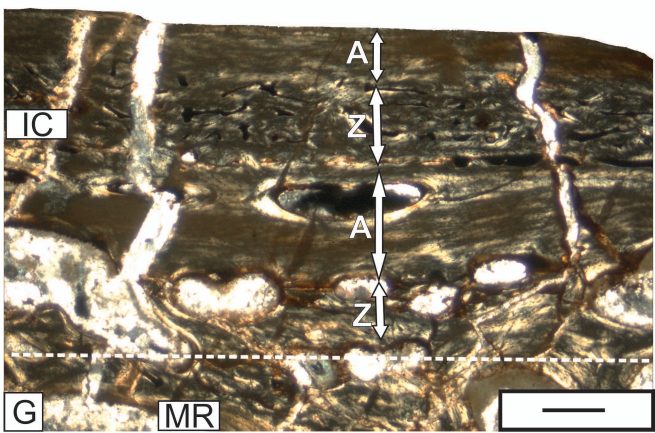

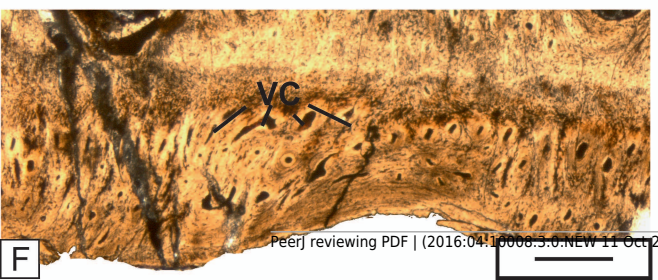

Figure 7 (on next page)

Histological details of the quadrate (A-C) and exoccipital (D-H) of *Metoposaurus krasiejowensis* skull (UOPB 01029) from the Late Triassic of Poland.

(A) Fragment of cortex of the quadrate; **(B)** The same as (A), but in cross-polarized light; **(C)** Trabecular bone of the quadrate bone; **(D)** Fragment of cortex of the exoccipital with distinct Sharpey's fibers; **(E)** Close-up of (D), note that the Sharpey's fibers are also visible in plane-polarized light; **(F)** The same as (E) but in cross-polarized light. Both images (E) and (F) are rotated clockwise for better arrangement of the figures; **(G)** Trabeculae visible in the central part of the exoccipital; **(H)** Remains of calcified cartilage preserved in the trabeculae part of exoccipital. Images (A), (C), (E), and (G) in plane-polarized light, others in cross-polarized light. Scale bars equal 500 µm for (C), (D) and (G), and 100 µm for other photographs. Abbreviations: C = cortex, CC = calcified cartilage, ER = erosion cavities, LB = lamellar bone, OL = osteocyte lacunae, PO = primary osteons, PFL = parallel-fibered bone, SO = secondary osteons, SF = Sharpey's fibers, TR = trabecular region, VC = vascular canals.